

1 Chemical composition, structures, and light absorption of N-containing
2 aromatic compounds emitted from burning wood and charcoal in
3 household cookstoves

4 Mingjie Xie¹, Zhenzhen Zhao¹, Amara L. Holder², Michael D. Hays², Xi Chen², Guofeng Shen³,
5 James J. Jetter², Wyatt M. Champion⁴, Qin'geng Wang⁵

6
7 ¹Collaborative Innovation Center of Atmospheric Environment and Equipment Technology,
8 Jiangsu Key Laboratory of Atmospheric Environment Monitoring and Pollution Control, School
9 of Environmental Science and Engineering, Nanjing University of Information Science &
10 Technology, 219 Ningliu Road, Nanjing 210044, China

11 ²Office of Research and Development, U.S. Environmental Protection Agency, 109 T.W.
12 Alexander Drive, Research Triangle Park, NC 27711, USA

13 ³Laboratory for Earth Surface Processes, College of Urban and Environmental Sciences, Peking
14 University, Beijing 100871, China

15 ⁴Oak Ridge Institute for Science and Education (ORISE) Postdoctoral Fellow at U.S.
16 Environmental Protection Agency, Office of Research and Development, Air Methods and
17 Characterization Division, 109 T.W. Alexander Drive, Research Triangle Park, NC 27711, USA

18 ⁵State Key Laboratory of Pollution Control and Resource Reuse, Nanjing University, Nanjing
19 210023, China

20
21 *Correspondence to:* Mingjie Xie

22 Email: mingjie.xie@colorado.edu; mingjie.xie@nuist.edu.cn

23 Tel: +1-18851903788;

24 Fax: +86-25-58731051;

25 Mailing address: 219 Ningliu Road, Nanjing, Jiangsu, 210044, China

26

27 **Abstract**

28 N-containing aromatic compounds (NACs) are an important group of light-absorbing
29 molecules in the atmosphere. They are often observed in combustion emissions, but their chemical
30 formulas and structural characteristics remain uncertain. In this study, red oak wood and charcoal
31 fuels were burned in cookstoves using the standard water boiling test (WBT) procedure.
32 Submicron aerosol particles in the cookstove emissions were collected using quartz (Q_f) and
33 polytetrafluoroethylene (PTFE) filter membranes positioned in parallel. A back-up quartz filter
34 (Q_b) was also installed downstream of the PTFE filter to evaluate the effect of sampling artifact on
35 NACs measurements. Liquid chromatography-mass spectroscopy (LC-MS) techniques identified
36 seventeen NAC chemical formulas in the cookstove emissions. The average concentrations of total
37 NACs in Q_b samples ($0.37 \pm 0.31 - 1.79 \pm 0.77 \mu\text{g m}^{-3}$) were greater than 50% of those observed
38 in the Q_f samples ($0.51 \pm 0.43 - 3.91 \pm 2.06 \mu\text{g m}^{-3}$), and the Q_b to Q_f mass ratios of individual
39 NACs had a range of 0.02 – 2.71, indicating that the identified NACs might have substantial
40 fractions remaining in the gas-phase. In comparison to other sources, cookstove emissions from
41 red oak or charcoal fuels did not exhibit unique NAC structural features, but had distinct NACs
42 composition. However, before identifying NACs sources by combining their structural and
43 compositional information, the gas-particle partitioning behaviors of NACs should be further
44 investigated. The average contributions of total NACs to the light absorption of organic matter at
45 $\lambda = 365 \text{ nm}$ (1.10 – 2.57%) in Q_f and Q_b samples (10.7 – 21.0%) are up to 10 times larger than
46 their mass contributions (Q_f 0.31 – 1.01%, Q_b 1.08 – 3.31%), so the identified NACs are mostly
47 strong light absorbers. To explain more sample extracts absorption, future research is needed to
48 understand the chemical and optical properties of high molecular weight (e.g., $\text{MW} > 500 \text{ Da}$)
49 entities in particulate matter.

50

51 **1 Introduction**

52 In the developing world, 2.8 billion people burn solid fuels in household cookstoves for
53 domestic activities such as heating and cooking (Bonjour et al., 2013). A variety of gaseous and
54 particle-phase pollutants — carbon monoxide (CO), nitrogen oxides (NO_x), volatile organic
55 compounds (VOCs), fine particulate matter with aerodynamic diameter $\leq 2.5 \mu\text{m}$ (PM_{2.5}), black
56 carbon (BC), organic carbon (OC), etc. — are emitted from cookstoves largely due to incomplete
57 combustion (Jetter et al., 2012; Shen et al., 2012; Wathore et al., 2017). In China, the relative
58 contributions of residential coal and biomass burning (BB) to annual PM_{2.5} emissions decreased
59 from 47% (4.32 Tg) in 1990 to 34% (4.39 Tg) in 2005 due to the growth in industrial emissions
60 (Lei et al., 2011). Although, more than half of BC (> 50 %) and OC (> 60 %) emissions are
61 attributed to residential coal and BB in both China and India (Cao et al., 2006; Klimont et al., 2009;
62 Lei et al., 2011).

63 Household solid fuel combustion is a leading human health risk, especially for women and
64 children who tend to spend more time indoors than men (Anenberg et al., 2013). Estimates show
65 that exposures to PM_{2.5} from domestic solid fuel combustion caused 3.9 million premature deaths
66 and ~4.8% of lost healthy life years (Smith et al., 2014). In addition, the emissions of carbonaceous
67 aerosols from cookstoves can affect the Earth's radiative balance by absorbing and scattering
68 incoming solar radiation (Lacey and Henze, 2015; Aunan et al., 2009). BC is the most efficient
69 light absorber in the atmosphere, while the total aerosol absorption, including that from OC, is still
70 highly uncertain (Yang et al., 2009; Park et al., 2010; Feng et al., 2013; Wang et al., 2014; Tuccella
71 et al., 2020). Multiple field and laboratory studies have demonstrated that OC in both primary PM
72 emissions (e.g., biomass and fossil fuel combustions) and secondary organic aerosol (SOA) feature
73 a range of absorptivity in the near ultraviolet (UV) and short visible wavelength regions

74 (Nakayama et al., 2010; Forrister et al., 2015; Lin et al., 2015; De Haan et al., 2017; Xie et al.,
75 2017a, b, 2018). The light absorbing OC fraction is often referred to as “brown carbon” (BrC).
76 Unlike open BB (e.g., forest, grassland, and cropland fires) — one of the most important primary
77 sources for organic aerosols (Bond et al., 2004) — the light absorption of BrC from household
78 cookstove emissions is rarely investigated. Sun et al. (2017) found that the BrC absorption from
79 residential coal burning accounted for 26.5% of the total aerosol absorption at 350~850 nm. BrC
80 from wood combustion in cookstoves has a greater mass specific absorption than that from open
81 BB over the wavelength range of 300 – 550 nm (Xie et al., 2018). These results suggest that
82 cookstove emissions may also be an important BrC source, which needs to be accounted for
83 separately from open BB.

84 Organic molecular markers (OMMs) are commonly used in receptor-based source
85 apportionment of carbonaceous aerosols (Jaeckels et al., 2007; Shrivastava et al., 2007; Xie et al.,
86 2012). Polycyclic aromatic hydrocarbons (PAHs) and their derivatives are a group of OMMs with
87 light absorption properties dependent on ring number or the degree of conjugation (Samburova et
88 al., 2016). As discussed in Xie et al. (2019), PAHs are generated from a multitude of combustion
89 processes (e.g., BB, fossil fuel combustion) (Chen et al., 2005; Riddle et al., 2007; Samburova et
90 al., 2016), and their ubiquitous nature makes them less than ideal OMMs for BrC source attribution.
91 Because of the specific toxicological concern raised by PAHs — they are mutagenic and
92 carcinogenic [International Agency for Research on Cancer (IARC), 2010] — source emission
93 factors (EFs), ambient levels, and potential health effects of PAHs are investigated exhaustively
94 (Ravindra et al., 2008; Kim et al., 2013). Similar to PAHs, N-containing aromatic compounds
95 (NACs) are a group of BrC chromophores commonly detected in ambient PM and source
96 emissions. Zhang et al. (2013) and Teich et al. (2017) calculated the absorption of individual NACs

97 in aqueous extracts of ambient PM, the total of which explained ~3% of the bulk extract absorption
98 at 365 – 370 nm. With the same approach, Xie et al. (2017a, 2019) found that the absorbance due
99 to NACs in BB or secondary OC was 3 – 10 times higher than their mass contributions. Lin et al.
100 (2016, 2017) estimated an absorbance contribution of 50 – 80% from NACs in BB OC directly
101 from their high-performance liquid chromatography (HPLC)/photodiode array (PDA) signals,
102 which are subject to considerable uncertainty due to the co-elution of other BrC chromophores
103 (e.g., PAHs and their derivatives). These results indicate that NACs are strong BrC chromophores,
104 but the estimation of their contributions to BrC absorption depends largely on how well they are
105 chemically characterized. Nitrophenols, methyl nitrophenols, nitrocatechols and methyl
106 nitrocatechols (including isomers) are typical atmospheric NACs (Claeys et al., 2012; Desyaterik
107 et al., 2013; Zhang et al., 2013). These NACs can be generated from BB (Lin et al., 2016, 2017;
108 Xie et al., 2019), fossil fuel combustion (Lu et al., 2019), and the reactions of aromatic volatile
109 organic compounds (VOCs) with reactive nitrogen species (e.g., NO_x) (Xie et al., 2017a), and are
110 not unique to specific sources (e.g., BB). By using a HPLC interfaced to a diode array detector
111 (DAD) and quadrupole (Q) time-of-flight mass spectrometer (ToF-MS), Xie et al. (2019) found
112 that BB NACs contain methoxy and cyanate groups. Nitronaphthol, nitrobenzenetriol, and methyl
113 nitrobenzenetriol are characteristic NACs for NO_x-based chamber reactions of naphthalene,
114 benzene, and *m*-cresol, respectively (Xie et al., 2017a). Yet, few studies have investigated the
115 composition of NACs from household cookstove emissions (Fleming et al., 2018; Lu et al., 2019).

116 The present study aims to characterize NACs in PM_{2.5} from burning red oak and charcoal in
117 a variety of cookstoves and calculate their contributions to bulk OC absorption. The absorption of
118 OC in solvent extracts of cookstove emissions were measured in our previous work (Xie et al.,
119 2018). Presently, NACs are identified and quantified using an earlier described HPLC/DAD-Q-

120 ToF-MS system. In addition, the NACs adsorbed on a backup quartz filter downstream of a
121 polytetrafluoroethylene (PTFE) membrane filter are analyzed, to evaluate the potential for
122 sampling artifacts of PM_{2.5} NACs on the bare quartz filter in parallel. This work unveils BrC
123 composition at a molecular level and increases the understanding of BrC chromophores and their
124 sources. It also shows that further identification of large molecules (e.g., > 500 Da) may better
125 explain BrC absorption in the particle phase.

126 **2 Methods**

127 *2.1. Cookstove emissions sampling*

128 The cookstove emission test facility, fuel-cookstove combinations, water boiling test (WBT)
129 protocol, and PM_{2.5} emissions sampling were described previously in Jetter and Kariher (2009)
130 and Jetter et al. (2012). Briefly, the cookstove emission tests were performed at the United States
131 Environmental Protection Agency (US EPA) cookstove test facility in Research Triangle Park,
132 NC, USA. Red oak wood and lump charcoal were burned in fuel-specific cookstoves under
133 controlled conditions. Emissions tests for each fuel-cookstove combination were performed in
134 triplicate. The WBT protocol (version 4) (Global Alliance for Clean Cookstoves, 2014) is designed
135 to measure cookstove power, energy efficiency, and fuel use, and contains cold-start (CS) high
136 power, hot-start (HS) high power, and simmer (SIM) low power phases. Both CS and HS phases
137 are defined by the duration between the ignition and the water boils. The CS phase starts with the
138 cookstove, pot, and water at ambient temperature; the HS immediately follows the CS with the
139 cookstove hot but the pot and water at ambient temperature; and the SIM phase is defined by a 30-
140 min time period with the cookstove hot and water temperature maintained at 3 °C below the boiling
141 point. Low moisture (~10%) oak and charcoal fuels were burned with five specific-designed
142 cookstove types (Tables S1 and S2); high moisture (~30%) oak fuels were burned in one cookstove

143 (Jiko Poa, BURN Manufacturing, Kenya). A brief description of each fuel-specific cookstove was
144 given in supplementary information (Text S1). Gaseous pollutant (e.g., CO, methane (CH₄))
145 emissions were monitored continuously, and PM_{2.5} filter samples were collected during each test
146 phase of the WBT protocol. The modified combustion efficiency (MCE), defined as CO₂/(CO₂ +
147 CO) on a molar basis, was calculated and discussed in Xie et al. (2018). A quartz-fiber filter (Q_f)
148 and a PTFE membrane filter positioned in parallel collected PM_{2.5} isokinetically at a flow rate of
149 16.7 L min⁻¹. The adsorption artifact of Q_f was evaluated using a quartz-fiber back-up filter (Q_b)
150 installed downstream of the PTFE filter during PM_{2.5} sampling.

151 **2.2. Chemical analysis**

152 The OC and elemental carbon (EC) emissions and UV-Vis light absorption properties (BrC)
153 of methanol-extracted cookstove particles were reported in Xie et al. (2018). Details for
154 determinations of OCEC concentrations and BrC absorption were provided in supplementary
155 information (Text S2). Except the 3-stone fire, EFs of OC and EC at the SIM phase were
156 substantially lower than those at high power phases (CS and HS), so the BrC absorption from red
157 oak and charcoal burning were primarily measured for CS- and HS-phase samples in Xie et al.
158 (2018). The SIM-phase samples were analyzed only for red oak burning in a 3-stone fire. This test
159 had comparable OC emissions between CS- and SIM-phase combustions, and CS and HS phases
160 of the 3-stone fire were typically similar and could not be separated (Xie et al., 2018). In the current
161 work, the same emission samples were selected for the analysis of NACs, and the three SIM-phase
162 samples from the 3-stone fire were treated as HS-phase samples of other cookstove tests. Tables
163 S1 and S2 summarized the measurement results of Q_f and Q_b, respectively, for each fuel-cookstove
164 combination, including concentrations of carbon contents and light-absorbing properties of sample
165 extracts. As the light absorption of BB BrC is expected to depend largely on burn conditions (Saleh

166 et al., 2014; Pokhrel et al., 2016), the MCE and EC/OC ratio, two indicators of burn conditions,
167 are also given in Table S1.

168 The Q_f and Q_b sample extraction and subsequent analysis for NACs were conducted as
169 described in Xie et al. (2019). In brief, an aliquot of each filter sample was pre-spiked with 250 ng
170 nitrophenol-d4 (internal standard) and extracted ultrasonically twice for 15 min in 3-5 mL of
171 methanol. After filtration (30 mm diameter \times 0.2 μ m pore size, PTFE filter, National Scientific Co.
172 Ltd, TN, USA), the extract volume was reduced to \sim 500 μ L with rotary evaporation prior to
173 HPLC/DAD-MS (Q-ToF) analysis. The NACs targeted in this work were chromatographed using
174 an Agilent 1200 Series HPLC equipped with a Zorbax Eclipse Plus C18 column (2.1 mm \times 100
175 mm, 1.8 μ m particle size; Agilent Technologies, CA, USA). The gradient separation was
176 performed using water (eluent A) and methanol (eluent B) containing 0.2% acetic acid (v/v) with
177 a total flow rate of 0.2 mL min⁻¹. The eluent B fraction was held at 25% for 3 min, increased to
178 100% over the next 7 min, where it was held for 22 min, and then returned to 25% over 5 min. An
179 Agilent 6520 Q-ToF MS equipped with a multimode ion source operating in electrospray
180 ionization (ESI) negative (-) mode was used to determine the chemical formula, molecular weight
181 (MW), and quantity of each target compound. All sample extracts were analyzed in full scan mode
182 over 40–1000 Da. A mass accuracy of \pm 10 ppm was selected for compound identification and
183 quantification. Samples with individual NACs exhibiting the highest MS signal intensities in full
184 scan mode were re-examined in targeted MS-MS mode using a collision-induced dissociation
185 (CID) technique. The MS-MS spectra of target NACs $[M-H]^-$ ions were acquired to deduce
186 structural information. Similar to bulk carbon and light absorption measurements, NACs were
187 primarily determined for CS- and HS-phase samples with substantial OC loadings.

188 Due to the limited availability of authentic standards, many of the NACs identified in
189 cookstove combustion samples were quantified using surrogate compounds with similar MW or
190 structures. An internal standard method with a 9-point calibration curve ($\sim 0.01 - 2 \text{ ng } \mu\text{L}^{-1}$) was
191 applied for quantification of concentrations. The compounds represented by each identified NAC
192 formula were quantified individually and combined to calculate the mass ratio of total NACs to
193 OC ($\mu\text{g m}^{-3}$) $\times 100\%$ (tNAC_{OC}%). Presently, the organic matter (OM) to OC ratio was not
194 measured or estimated for cookstove combustion emissions, so tNAC_{OC}% could be up to 2 times
195 greater than the contributions of NACs to OM (Reff et al., 2009; Turpin and Lim, 2001). Table S3
196 lists the chemical formulas, proposed structures, and standard assignments for the NACs identified
197 here. The quality assurance and control (QA/QC) procedures for filter extraction and instrumental
198 analysis were the same as Xie et al. (2017a, 2019). NACs were not detected in field blank and
199 background samples. The average recoveries of NAC standards on pre-spiked blank filters ranged
200 from 75.1% to 116%, and the method detection limit had a range of 0.70–17.6 pg.

201 **2.3. Data analysis**

202 In Xie et al. (2017a), the DAD measurement directly identified the chemical compounds in
203 chamber SOA responsible for light absorption in the near UV and visible light ranges. However,
204 no light absorption from individual NACs was detected in the DAD chromatograms from open BB
205 (Xie et al., 2019) and cookstove emissions (this work). So the contributions of individual NACs
206 to light absorption coefficient (Abs_{λ} , Mm^{-1}) for each sample extract at 365 nm ($\text{Abs}_{365, \text{iNAC}}\%$) were
207 calculated using the method described in Xie et al. (2017a, 2019):

$$208 \text{Abs}_{365, \text{iNAC}}\% = \frac{C_{\text{iNAC}} \times \text{MAC}_{365, \text{iNAC}}}{\text{Abs}_{365}} \times 100\% \quad (1)$$

209 where C_{iNAC} is the mass concentration (ng m^{-3}) of individual NACs, and $\text{MAC}_{365, \text{iNAC}}$ is the mass
210 absorption coefficient (MAC_{λ} , $\text{m}^2 \text{g}^{-1}$) of individual NACs at 365 nm. Abs_{365} is the light absorption

211 coefficient (Mm^{-1}) of each sample extract at 365 nm, and has been widely used to represent BrC
212 absorption (Chen and Bond, 2010; Hecobian et al., 2010; Liu et al., 2013). Each NAC compound
213 was assumed to absorb as a standard (Table S3), of which the $\text{MAC}_{365,\text{iNAC}}$ value was obtained
214 from Xie et al. (2017a, 2019) and listed in Table S4. In this work, Student's t -test was used to
215 determine if the means of two sets of data are significantly different from each other, and a p value
216 less than 0.05 indicates significant difference.

217 **3 Results and discussion**

218 *3.1 Summary of total NACs concentration from cookstove emissions*

219 Table 1 summarizes the average concentrations of total NACs and average $\text{tNAC}_{\text{OC}\%}$ for
220 Q_f and Q_b by fuel type and WBT phase. The EFs of total NACs shown in Table S5 were obtained
221 by multiplying the EFs of OC and $\text{tNAC}_{\text{OC}\%}$. Filter samples of emissions from burning red oak
222 wood had significantly ($p < 0.05$) higher average total NAC concentrations and $\text{tNAC}_{\text{OC}\%}$ than
223 the charcoal burning samples. Wood burning generates more volatile aromatic compounds (e.g.,
224 phenols, PAHs) than charcoal burning (Kim Oanh, et al., 1999), and NACs can form when
225 aromatic compounds and reactive nitrogen (e.g., NO_x) are present during solid fuel combustion
226 (Lin et al., 2016, 2017). While burning red oak, emissions from the CS and HS phases show similar
227 average NAC concentrations, $\text{tNAC}_{\text{OC}\%}$, and NAC EFs (Tables 1 and S5). Additionally, burning
228 low moisture red oak in the Jiko Poa stove had higher $\text{tNAC}_{\text{OC}\%}$ than burning high moisture red
229 oak (Tables S6 and S7), but the difference was not significant ($p > 0.05$). Thus, the NAC emissions
230 from red oak burning are less likely influenced by WBT phase, and the effect of fuel moisture
231 content needs further investigation. For charcoal fuel samples, compared with the CS-phase, the
232 HS-phase shows significantly higher ($p < 0.05$) average NAC concentrations and EFs. This is

233 likely due to the increase in OC with the HS phase (Tables 1 and S5), as the average tNACoc%
234 values are much closer for the CS- ($0.40 \pm 0.25\%$) and HS-phases ($0.31 \pm 0.21\%$).

235 Several studies have placed a quartz-fiber filter behind a PTFE filter to evaluate the positive
236 adsorption artifact — adsorption of gas-phase compounds onto particle filter media, “blow-on”
237 effect (Peters et al., 2000; Subramanian et al., 2004; Watson et al., 2009; Xie et al., 2014). This
238 method is expected to provide a consistent estimate irrespective of sampling time, but may over
239 correct the positive artifact by 16–20% due to volatilization of OC off the upstream PTFE filter
240 (negative artifact, “blow-off” effect) (Subramanian et al., 2004). A denuder upstream of the filter
241 for gas sampling was used to avoid positive artifact in several studies (Ding et al., 2002; Ahrens
242 et al., 2012). This approach can generate large negative artifacts by altering the gas-particle
243 equilibrium after the denuder, and a denuder efficiency of 100% might not be guaranteed
244 (Kirchstetter et al., 2001; Subramanian et al., 2004). The present study is the first to consider
245 sampling artifact when measuring semivolatile NACs. This concept merits consideration as
246 quantification of particle-phase NACs may be subject to large uncertainty. Table 1 shows that the
247 average concentrations of total NACs on Q_b ($0.37 \pm 0.31 - 1.79 \pm 0.77 \mu\text{g m}^{-3}$) are greater than
248 50% and 80% of those on Q_f ($0.51 \pm 0.43 - 3.91 \pm 2.06 \mu\text{g m}^{-3}$) for red oak and charcoal burning,
249 respectively. The average Q_b to Q_f ratio in percentage using OC concentrations is 2-3 times lower
250 ($14.8 \pm 3.87 - 38.8 \pm 18.9\%$). Hence, the NACs identified in this work are present in the relatively
251 volatile bulk OC fraction emitted from cookstoves, and the NACs in the Q_f samples may also be
252 present in the gas-phase in the atmosphere. Charcoal burning emissions show even higher ($p < 0.05$)
253 Q_b to Q_f total NAC mass ratios (CS $84.1 \pm 38.0\%$, HS $140 \pm 52.9\%$) than red oak burning (CS 50.8
254 $\pm 13.4\%$, HS $53.4 \pm 26.2\%$), which is largely due to the higher OC loads on Q_f from red oak
255 burning. Xie et al. (2018) assumed previously that the Q_b -adsorbed OC represented the positive

256 sampling artifact only, and adjusted the light absorbing properties of OC on Q_f by subtracting
257 Abs_{365} and OC of Q_b samples directly. In this study, the high Q_b to Q_f ratios of total NACs indicate
258 that the volatilization of NACs from upstream PTFE filter cannot be neglected, but the relative
259 contributions of positive and negative artifacts to Q_b measurements are unknown. Therefore, the
260 measurement results of NACs in Q_f and Q_b samples were provided separately, and no correction
261 was conducted for Q_f measurements in this work. Since the gaseous NACs adsorbed in Q_b samples
262 depends on Q_f loadings, $tNAC_{OC}\%$ and total NACs concentrations in each Q_f - Q_b pair from
263 matching tests are significantly correlated ($p < 0.05$, Fig. S1a, b, d, and e).

264 Along with modified combustion efficiency (MCE), the EC/OC and BC/OA (organic
265 aerosol) ratios were used previously as indicators of biomass burning conditions (McMeeking et
266 al., 2014; Pokhrel et al., 2016). Here the burn condition indicates general flame intensity or
267 combustion temperature (Chen and Bond, 2010; Saleh et al., 2014), and is parameterized to
268 investigate combustion processes (e.g., pyrolysis). The MCE, EC/OC and BC/OA ratios are key
269 to understanding particulate OC absorptivity (Saleh et al., 2014; Lu et al., 2015) and NACs
270 formation from open BB (Xie et al., 2019). Presently, the relationships of $tNAC_{OC}\%$ versus EC/OC
271 for Q_f samples are shown in Fig. S1c and f by fuel type. Because no significant difference was
272 observed for average total NACs concentrations, $tNAC_{OC}\%$, and EC/OC ratios when testing CS-
273 versus HS- phases during red oak fuel burning, the CS- and HS-phases were pooled for a regression
274 analysis. The $tNAC_{OC}\%$ of Q_f samples positively correlate ($r = 0.83$, $p < 0.05$) with EC/OC for red
275 oak burning (Fig. S1c), as observed in Xie et al. (2019) for open BB, which suggests that burn
276 conditions influence NACs formation during BB. Note that the NAC concentrations on Q_f were
277 possibly adsorbed while in a gaseous state, while EC is particle phase.

278 In Table S1, the MCE values of charcoal burning indicate that the HS-phase is more
279 smoldering than the CS-phase. However, the average $tNAC_{OC}\%$ values showed no significant
280 difference ($p = 0.29$) between HS and CS phases. Like MAC_{365} and \dot{A}_{abs} in Q_f samples for charcoal
281 burning (Xie et al., 2018), $tNAC_{OC}\%$ derived from the same samples did not correlate with EC/OC
282 ratios in this work (Fig. S1f). Xie et al. (2018) found that the HS-phase for charcoal burning had
283 average OC EFs 5–10 times higher than the CS-phase, while the EC EFs decreased by more than
284 90% from the CS- to HS-phase. Furthermore, no correlation has been observed between MCE and
285 EC/OC for charcoal burning at the HS-phase. So, the EC/OC for charcoal burning tends to depend
286 more on the initial temperature in the cookstove than MCE variations, and cannot be used to predict
287 burn conditions, BrC absorption, or NACs formation.

288 **3.2 Composition of NACs in Q_f and Q_b**

289 During solid fuel combustion, NACs may form from aromatic compounds (e.g., substituted
290 phenols) and reactive nitrogen species (e.g., NH_3 , NO_x , and HONO) in both the gas- and particle-
291 phase (Harrison et al., 2005; Kwamena and Abbatt, 2008; Lu et al., 2011; Lin et al., 2016, 2017).
292 Aromatic hydrocarbons are produced during fuel pyrolysis (Simoneit et al., 1993; Simoneit, 2002;
293 Kaal et al., 2009). Oxidation of fuel derived nitrogen, rather than molecular nitrogen in air, is the
294 major formation pathway of reactive nitrogen species (Glarborg et al., 2003).

295 Presently, seventeen chemical formulas were identified as NACs in cookstove emissions,
296 several of which are widely observed in ambient air and open BB particles (e.g., $C_6H_5NO_3$,
297 $C_6H_5NO_4$) (Claeys et al., 2012; Zhang et al., 2013; Lin et al., 2016, 2017; Xie et al., 2019). Figure
298 1 shows the average concentrations ($ng\ m^{-3}$) of individual NACs in Q_f and Q_b samples by fuel type
299 and WBT phase. The corresponding average mass ratios of individual NACs to $OC \times 100\%$

300 (iNAC_{OC}%) are exhibited in Fig. S2. Details of the NACs composition expressed in iNAC_{OC}% for
301 each fuel-cookstove experiment are given in Tables S6–S9.

302 Generally, the CS and HS phases have consistent NAC profiles for red oak combustion
303 (Figs. 1a, b and S2a, b). C₁₀H₇NO₃ (CS-Q_f 1003 ± 803 ng m⁻³, HS-Q_f 1149 ± 1053 ng m⁻³) and
304 C₈H₅NO₂ (CS-Q_f 712 ± 921 ng m⁻³, HS-Q_f 1185 ± 1761 ng m⁻³) have the highest average
305 concentrations on Q_f, followed by C₁₁H₉NO₃, C₁₀H₁₁NO₅, and C₁₁H₁₃NO₅. However, C₈H₅NO₂
306 was only detected in emission samples of Jiko Poa among the five wood stoves (Tables S6 and
307 S7). Not considering C₈H₅NO₂, Q_b samples of red oak combustion emissions have similar NACs
308 profiles and characteristic species (e.g., C₁₀H₇NO₃, C₁₁H₉NO₃) as Q_f samples, and the individual
309 NAC distributions in Q_b to Q_f samples are similar between the CS- and HS-phases (Fig. 1a, b). It
310 appears that the formation of NACs from red oak burning in cookstoves depends largely on burn
311 conditions reflected by EC/OC ratios (Fig. S1c) rather than WBT phases. Among the 17 identified
312 NACs from red oak burning, C₈H₅NO₂ and C₁₁H₁₃NO₆ have the lowest Q_b to Q_f ratios (2.03 –
313 9.80%, Fig. 1a, b), indicating their low volatility. The low volatility of C₁₁H₁₃NO₆ might be due
314 to its relatively high MW; while C₈H₅NO₂ has the second lowest MW and its structure likely
315 contains functional groups that decrease vapor pressure (e.g., carboxyl group) (Donahue et al.,
316 2011).

317 Charcoal burning generated high abundances of C₈H₉NO₅, C₁₁H₉NO₃, and C₁₀H₇NO₃ for
318 both CS (86.6 ± 98.7 – 170 ± 200 ng m⁻³) and HS (97.1 ± 38.5 – 178 ± 104 ng m⁻³) phases (Figs.
319 1c, d and S2c, d). Only one of the five charcoal stoves (Éclair, GIZ, Bonn, Germany) emitted
320 C₈H₅NO₂, which was not detected on Q_b for charcoal combustions (Tables S8 and S9). Average
321 concentrations of C₈H₉NO₅, C₁₁H₉NO₃, and C₁₀H₇NO₃ in the Q_b (62.0 ± 64.9 – 198 ± 115 ng m⁻³)
322 and Q_f samples were comparable. However, the iNAC_{OC}% of these compounds are 1.45 ± 0.68 –

323 5.16 ± 2.84 times higher in Q_b (iNAC_{OC}%, $0.11 \pm 0.18 - 0.46 \pm 0.69\%$) than in Q_f samples (0.052
324 $\pm 0.067 - 0.14 \pm 0.15\%$). High levels of $C_6H_5NO_4$, $C_7H_7NO_4$, and $C_8H_9NO_4$ were also observed in
325 the HS phase for charcoal burning (Fig. 1d). These compounds in Q_b samples had average
326 concentrations ($222 \pm 132 - 297 \pm 277 \text{ ng m}^{-3}$) $22.6 - 80.8\%$ higher than in Q_f samples (150 ± 118
327 $- 181 \pm 111 \text{ ng m}^{-3}$). As such, the charcoal HS phase generates more low MW NACs (e.g.,
328 $C_6H_5NO_4$, $C_7H_7NO_4$) than the CS phase, and the initial temperature in the cookstove has an impact
329 on NAC formation from charcoal burning.

330 As mentioned in section 3.1, using a Q_b has been widely applied to evaluate the positive
331 sampling artifact for OC and semivolatile organic compounds. This method might only work for
332 bulk PM, OC, and low volatile organic compounds, of which the concentrations in Q_b samples are
333 much lower than Q_f samples and usually presumed to be due to positive adsorption artifacts only
334 (Subramanian et al., 2004; Watson et al., 2009). In this work, the average Q_b to Q_f mass ratios of
335 the 17 individual NACs ranged from $50.8 \pm 13.4\%$ to $140 \pm 52.9\%$, comparable to *n*-alkanes with
336 carbon number ≤ 21 (e.g., heneicosane; $26.3 - 163\%$) and PAHs with benzene ring number ≤ 4 (e.g.,
337 fluoranthene; $46.3 - 134\%$) in the ambient of urban Denver (Xie et al., 2014). Xie et al. (2014)
338 found that the gas-phase concentrations of *n*-alkanes and PAHs with vapor pressure greater than
339 heneicosane and fluoranthene were comparable or higher than their particle-phase concentrations.
340 The vapor pressure of five NACs standards at $25 \text{ }^\circ\text{C}$ ($p^{0,*}_L$) were predicted using the US EPA
341 Toxicity Estimation Software Tool (T.E.S.T) and listed in Table S10. Their $p^{0,*}_L$ values are mostly
342 higher than heneicosane and fluoranthene ($\sim 10^{-8}$ atm; Xie et al., 2013, 2014). Then the identified
343 NACs in this study may have substantial fractions remaining in the gas phase. As the evaporation
344 of NACs from the upstream filter (negative artifact) is unknown, the particle-phase NAC
345 concentrations cannot be calculated by simply subtracting Q_b measurements from those of Q_f .

346 Considering that most of the Q_f and Q_b samples were collected near ambient temperature (Table
347 S2, ~ 25 °C), the composition of NACs derived from Q_f measurements alone can be biased due to
348 the lack of gas-phase measurements. Future work is needed to evaluate the composition of NACs
349 from emission sources in both the particle and gas phases.

350 ***3.3 Identification of NACs structures***

351 Figures S3 and S4 exhibited extracted ion chromatograms (EICs) and MS-MS spectra of
352 the 17 identified NACs. For comparison, the MS-MS spectra of standard compounds used in this
353 work are obtained from Xie et al. (2017a, 2019) and shown in Fig. S5. Among all identified NAC
354 formulas, $C_{10}H_7NO_3$ was detected in each fuel-cookstove experiment (Tables S6 – S9) and showed
355 the highest concentrations in emissions from burning red oak (Fig. 1a, b). The MS-MS spectrum
356 of $C_{10}H_7NO_3$ (Fig. S4l) is like 2-nitro-1-phenol (Fig. S5g) but shows a ~ 1 min difference in
357 retention time (Fig. S3i 10.9 min, 2-nitro-1-phenol 11.8 min). $C_{10}H_7NO_3$ is presumed to be an
358 isomer of 2-nitro-1-phenol with a nitronaphthol structure. $C_{11}H_9NO_3$ has a degree of unsaturation
359 and a fragmentation pattern (Fig. S4q) like $C_{10}H_7NO_3$ and is likely a structural isomer of methyl
360 nitronaphthol. $C_6H_5NO_3$, $C_7H_7NO_3$, $C_6H_5NO_4$, and $C_7H_7NO_4$ are commonly detected in
361 combustion emissions (Lin et al., 2016, 2017; Xie et al., 2019) and atmospheric particles (Claeys
362 et al., 2012; Zhang et al., 2013). $C_6H_5NO_3$ and $C_6H_5NO_4$ are identified as 4-nitrophenol and 4-
363 nitrocatechol using authentic standards (Figs. S4a, d and S5a, c). $C_7H_7NO_3$ has two isomers (Fig.
364 S3b) and the compound eluting at 9.98 min has the same retention time and MS-MS spectrum (Fig.
365 S4c) as 2-methyl-4-nitrophenol (Fig. S5b). In ambient PM and chamber SOA, $C_7H_7NO_4$ was
366 identified using standard compounds as a series of methyl-nitrocatechol isomers (4-methyl-5-
367 nitrocatechol, 3-methyl-5-nitrocatechol, and 3-methyl-6-nitrocatechol) (Iinuma et al., 2010).
368 According to the HPLC-Q-ToFMS data for $C_7H_7NO_4$ identified in Iinuma et al. (2010) and our

369 previous studies (Xie et al., 2017a, 2019), the two $C_7H_7NO_4$ isomers in Fig. S3d are likely 4-
370 methyl-5-nitrocatechol and 3-methyl-6-nitrocatechol, respectively. Here we cannot rule out the
371 presence of 3-methyl-5-nitrocatechol, which may co-elute with 4-methyl-5-nitrocatechol (Iinuma
372 et al., 2010). In Fig. S4k, o, and p, the MS-MS spectra of $C_7H_7NO_5$, $C_8H_7NO_5$, and $C_8H_9NO_5$ all
373 show a loss of $CH_3 + NO$ (or NO_2) + CO. The loss of CH_3 is typically due to a methoxy group in
374 NAC molecules, and NO (or NO_2) and CO loss is commonly observed for NACs with more than
375 one phenoxy group (Xie et al., 2019). So methoxy nitrophenol is the proposed skeleton for
376 $C_7H_7NO_5$, $C_8H_7NO_5$, and $C_8H_9NO_5$. Other functional groups were estimated using their chemical
377 formulas and degree of unsaturation as a basis (Table S3).

378 The present study quantifies $C_8H_7NO_4$ and $C_9H_9NO_4$ using 2-methyl-5-benzoic acid
379 ($C_8H_7NO_4$) and 2,5-dimethyl-4-nitrobenzoic acid ($C_9H_9NO_4$), respectively. The fragmentation
380 patterns of $C_8H_7NO_4$ (Fig. S4g, h) and $C_9H_9NO_4$ compounds (Fig. S4m, n) are different from their
381 corresponding surrogates (Fig. S5f, h) and loss of CO_2 is not observed, so $C_8H_7NO_4$ and $C_9H_9NO_4$
382 compound structures do not include a carboxyl group. The MS-MS spectra of $C_8H_7NO_4$ eluting at
383 8.14 min (Fig. S3e) and $C_9H_9NO_4$ eluting at 9.22 min (Fig. S3j) indicate the loss of OCN (Fig.
384 S4g, m), suggesting benzoxazole/benzisoxazole structure or the presence of cyanate ($-O-C\equiv N$) or
385 isocyanate ($-O=C=N$) groups. Mass spectra of selected standard compounds (Fig. S5i-n) in our
386 previous work (Xie et al. 2019) show the loss of an OCN group only happens during the
387 fragmentation of phenyl cyanate. Thus, the $C_8H_7NO_4$ and $C_9H_9NO_4$ isomers containing OCN
388 indicate a phenyl cyanate feature. However, the fragmentation mechanism related to the loss of a
389 single nitrogen for the second $C_8H_7NO_4$ isomer (Figs. S3e and S4h) is unknown and requires
390 further study. The MS-MS spectrum of the second $C_9H_9NO_4$ isomer had dominant ions at m/z 194
391 ($[M-H]^+$), 164 (loss of NO), and 149 (loss of NO + CH_3). Compared with the MS-MS spectra of

392 4-nitrophenol and 2-methyl-4-nitrophenol (Fig. S5a, b), the second $C_9H_9NO_4$ isomer is likely a
393 methoxy nitrophenol with an extra ethyl group.

394 The EIC signal of $C_8H_9NO_4$ in Fig. S3f comprises at least 3-4 isomers, and the MS-MS
395 spectra are always dominated by ions at m/z 182 ($[M-H]^-$), 152 (loss of NO), and 137 (loss of NO
396 + CH_3) with some changes in relative abundance. The fragmentation mechanism of $C_8H_9NO_4$
397 represented by the MS-MS spectrum in Fig. S4i is consistent with that of the second $C_9H_9NO_4$
398 isomer (Fig. S4n), so the $C_8H_9NO_4$ might also have a methoxy nitrophenol skeleton. The MS-MS
399 spectrum of $C_8H_5NO_2$ is characterized by CO_2 loss (Fig. S4j), indicative of a carboxyl group.
400 Considering the degree of unsaturation of the $C_8H_5NO_2$ molecule and the cyano group feature in
401 BB tracers (e.g., hydrogen cyanide, benzonitrile) (Schneider et al., 1997; Li et al., 2000; Gilman
402 et al., 2015), $C_8H_5NO_2$ was identified as 4-cyanobenzoic acid using authentic standard (Fig. S5o).
403 The $C_{10}H_{11}NO_4$, $C_{10}H_{11}NO_5$, $C_{11}H_{13}NO_5$, and $C_{11}H_{13}NO_6$ detected here are also observed in other
404 BB experiments (Xie et al., 2019). Their MS-MS spectra are characterized by the loss of at least
405 one CH_3 and/or OCN (Fig. S4r-u), suggestive of methoxy or cyanate groups. Without authentic
406 standards, fragmentation patterns (Fig. S4r-u) were used to determine the molecular structures of
407 $C_{10}H_{11}NO_4$, $C_{10}H_{11}NO_5$, $C_{11}H_{13}NO_5$, and $C_{11}H_{13}NO_6$ (Table S3).

408 Nearly all NAC formulas identified in this work were observed previously (Lin et al., 2016,
409 2017; Xie et al., 2017a; Fleming et al., 2018; Xie et al., 2019). Few studies attempt to retrieve
410 structural information for NACs using MS-MS spectra of authentic standards. Although multiple
411 NACs may be generated from BB and photooxidation of aromatics in the presence of NO_x , NAC
412 structures may differ across emission sources. Xie et al. (2019) found that fragmentation patterns
413 of $C_7H_7NO_5$ and $C_8H_9NO_5$ from BB and photochemical reactions are distinct, and the methoxy
414 and cyanate groups are featured only in BB NACs. Thus, knowing the NAC structure is useful to

415 emissions source identification. In this work, the chemical and structural information obtained for
416 NACs sampled during red oak and charcoal burning are similar, presumably because the charcoal
417 fuel used is produced by the slow pyrolysis of wood. However, NACs in red oak and charcoal
418 burning emissions can be differentiated compositionally. As shown in Figs. 1 and S2, the NAC
419 emissions from red oak burning in cookstoves are characterized by $C_{10}H_7NO_3$ and $C_{11}H_9NO_3$. In
420 addition to these two species, charcoal burning in cookstoves also generates high fractions of
421 $C_8H_9NO_5$ (Fig. S2c, d). This difference among NACs may help with source apportionment using
422 receptor models, which are commonly used and assume that the ambient pollutants measured in
423 the field are linear combinations from a number of time-variant sources/factors. (Jaeckels et al.,
424 2007; Shrivastava et al., 2007; Xie et al., 2013).

425 Figure 2 compares NAC composition from cookstove emissions (not including $C_8H_5NO_2$),
426 open BB (Xie et al., 2019), and SOA chamber experiments (Xie et al., 2017a). Since previous
427 source emissions studies ignored Q_b measurements and normalized individual NACs
428 concentrations to OM, only Q_f measurements in this work are compared (Fig. 2a, b) with their
429 $iNAC_{OC}\%$ values multiplied by 1.7 (proposed OM/OC ratio, Reff et al., 2009). The three open BB
430 tests (Fig. 2c) were conducted with two fuel types under different ambient temperatures (10–29
431 °C) and RH% (49–83%) (Xie et al., 2019). But they consistently emit $C_6H_5NO_4$, $C_7H_7NO_4$, and
432 $C_9H_9NO_4$, which is compositionally distinct from cookstove emissions (Fig. 2a, b). Moreover, the
433 average mass contribution of total NACs to OM for open BB ($0.12 \pm 0.051\%$) was 4–14 times
434 lower than that for cookstove emissions. This result is likely due to the high temperature flaming
435 combustion produced in the cookstoves (Shen et al., 2012; Xie et al., 2018). In Fig. 2d and e, the
436 NAC profiles yielded for photochemical reactions appear to have aromatic precursors. When using
437 field measurement data of NACs for receptor modeling, the resulting factors can be linked with

438 specific emission sources by comparing with the NAC patterns shown in Fig. 2. Further studies
439 are also warranted to unveil NAC patterns of other potential sources (e.g., motor vehicle emissions).
440 Therefore, the source of NACs can be identified by combining their characteristic structures and
441 composition. The filter-based NACs reported for the experiments shown in Fig. 2 were all
442 measured using the identical method and HPLC-Q-ToFMS instrument, reducing any potential
443 methodological bias. However, total gas-phase NAC concentrations need to be properly sampled
444 and measured to account for the impact of gas/particle partitioning on their distribution.

445 **3.4 Contributions of NACs to Abs₃₆₅**

446 The average Abs_{365,iNAC%} values of Q_f and Q_b samples are presented by fuel type and WBT
447 phase in the Fig. 3 stack plots, and experimental data for each fuel-cookstove are provided in
448 Tables S11–S14. The average contributions of total NACs to Abs₃₆₅ (Abs_{365,tNAC%}) of the sample
449 extracts (Q_f 1.10 – 2.57%, Q_b 10.7 – 21.0%) are up to 10 times greater than their average tNAC_{OC%}
450 (Q_f 0.31 – 1.01%, Q_b 1.08 – 3.31%, Table 1). Considering that some NACs are not light-absorbing
451 (Table S4) and the OM/OC ratio is typically greater than unity, most NACs that contribute to
452 Abs₃₆₅ are strong BrC chromophores. Like the mass composition of NACs (Fig. 1), C₁₀H₇NO₃ (CS
453 0.24%, HS 0.43%) and C₈H₉NO₅ (CS 1.22%, HS 0.55%) were the major contributors to Abs₃₆₅
454 for the Q_f samples collected during red oak and charcoal burning, respectively (Fig.3a). The
455 average Abs_{365,tNAC%} of Q_b samples are 7.53 to 11.3 times higher than those of Q_f samples. Unlike
456 the Q_f samples from red oak burning, C₁₀H₁₁NO₅ (CS 2.77%, HS 3.09%) has the highest average
457 contribution to Abs₃₆₅ for Q_b samples, followed by C₁₀H₇NO₃ (CS 1.96%, HS 1.32%) and
458 C₈H₉NO₅ (CS 1.32%, HS 1.44%). While C₈H₉NO₅ dominated the contribution (CS 8.78%, HS
459 5.82%) to Abs₃₆₅ for the Q_b samples from charcoal burning (Fig. 3b). All identified NACs
460 explained 1.10 – 2.58% (Fig. S3) of Q_f extracts absorption. Even if the NACs on Q_b were totally

461 derived from upstream filter evaporation, the adjusted average contributions of total NACs ($Q_f +$
462 Q_b) to Abs_{365} of Q_f extracts were still lower than 5% (1.59 – 4.01%). Due to the lack of authentic
463 standards, the quantification of NACs concentrations and their contributions to Abs_{365} of Q_f
464 extracts might be subject to uncertainties. However, growing evidences showed that BrC
465 absorption was majorly contributed by large molecules with $MW > 500 - 1000$ Da (Di Lorenzo
466 and Young, 2016; Di Lorenzo et al., 2017). Large molecules of NACs may be generated from
467 flaming combustions in cookstoves, and their structures and light absorption are worth future
468 investigations. In previous studies on ambient and biomass burning particles, most identified
469 NACs had a MW lower than 300 – 500 Da, and their total contributions to bulk BrC absorption
470 were estimated to be less than 10% (Mohr et al., 2013; Zhang et al., 2013; Teich et al., 2017; Xie
471 et al., 2019). Similar results were also obtained in the current work. Therefore, further studies are
472 needed to identify large BrC molecules (including high MW NACs) in ambient and source
473 particles.

474 **4 Conclusion**

475 This study investigated the composition, chemical formulas, and structures of NACs in
476 $PM_{2.5}$ emitted from burning red oak and charcoal in a variety of cookstoves. Total NAC mass and
477 compositional differences between Q_f and Q_b samples suggest that the identified NACs might have
478 substantial gas-phase concentrations. By comparing the MS-MS spectra of identified NACs to
479 standard compound spectra, the structures of NACs featuring methoxy and cyanate groups in
480 cookstove emissions are confirmed. The source identification of NACs would be less ambiguous
481 if both the structures and composition of NACs are known, as different emission sources have
482 distinct NAC characteristics. However, the compositional information of NACs based on Q_f
483 measurements only are biased due to the lack of gas-phase data, and further studies are warranted

484 to investigate the gas/particle distribution of NACs in the ambient and source emissions. Similar
485 to previous work, the average contribution of total NACs to Abs₃₆₅ of Q_f samples is less than 5%
486 (1.10 – 2.57%), suggesting the need to shift our focus from low MW NACs (MW < 300 Da) to the
487 chemical and optical properties of large molecules (e.g., MW > 500 Da) in particles.

488

489 *Data availability*

490 Data used in the writing of this manuscript is available at the U.S. Environmental Protection
491 Agency’s Environmental Dataset Gateway (<https://edg.epa.gov>).

492

493 *Competing interests*

494 The authors declare that they have no conflict of interest.

495

496 *Disclaimer*

497 The views expressed in this article are those of the authors and do not necessarily represent the
498 views or policies of the U.S. Environmental Protection Agency.

499

500 *Author contribution*

501 MX and AH designed the research. MX, ZZ, and XC performed the experiments. GS, WC, and JJ
502 managed cookstove emission tests and sample collection. MX and MH analyzed the data and wrote
503 the paper with significant contributions from AH and QW.

504

505 *Acknowledgements*

506 This research was supported by the National Natural Science Foundation of China (NSFC,
507 41701551), the Startup Foundation for Introducing Talent of NUIST (No. 2243141801001), and
508 in part by an appointment to the Postdoctoral Research Program at the Office of Research and
509 Development by the Oak Ridge institute for Science and Education through Interagency
510 Agreement No. 92433001 between the U.S. Department of Energy and the U.S. Environmental
511 Protection Agency. We thank B. Patel for assistance on ECOC analysis of PM_{2.5} filters.

512

513 **References**

- 514 Ahrens, L., Harner, T., Shoeib, M., Lane, D. A., and Murphy, J. G.: Improved characterization of gas-particle
515 partitioning for per- and polyfluoroalkyl substances in the atmosphere using annular diffusion denuder samplers,
516 *Environmental Science & Technology*, 46, 7199-7206, 10.1021/es300898s, 2012.
- 517 Anenberg, S. C., Balakrishnan, K., Jetter, J., Masera, O., Mehta, S., Moss, J., and Ramanathan, V.: Cleaner cooking
518 solutions to achieve health, climate, and economic cobenefits, *Environmental Science & Technology*, 47, 3944-
519 3952, 10.1021/es304942e, 2013.
- 520 Aunan, K., Berntsen, T. K., Myhre, G., Rypdal, K., Streets, D. G., Woo, J.-H., and Smith, K. R.: Radiative forcing
521 from household fuel burning in Asia, *Atmospheric Environment*, 43, 5674-5681,
522 <https://doi.org/10.1016/j.atmosenv.2009.07.053>, 2009.
- 523 Bond, T. C., Streets, D. G., Yarber, K. F., Nelson, S. M., Woo, J.-H., and Klimont, Z.: A technology-based global
524 inventory of black and organic carbon emissions from combustion, *Journal of Geophysical Research: Atmospheres*,
525 109, 10.1029/2003jd003697, 2004.
- 526 Bonjour, S., Adair-Rohani, H., Wolf, J., Bruce Nigel, G., Mehta, S., Prüss-Ustün, A., Lahiff, M., Rehfuess Eva, A.,
527 Mishra, V., and Smith Kirk, R.: Solid fuel use for household cooking: Country and regional estimates for 1980-
528 2010, *Environmental Health Perspectives*, 121, 784-790, 10.1289/ehp.1205987, 2013.
- 529 Cao, G., Zhang, X., and Zheng, F.: Inventory of black carbon and organic carbon emissions from China, *Atmospheric*
530 *Environment*, 40, 6516-6527, <https://doi.org/10.1016/j.atmosenv.2006.05.070>, 2006.
- 531 Chen, Y., Sheng, G., Bi, X., Feng, Y., Mai, B., and Fu, J.: Emission factors for carbonaceous particles and polycyclic
532 aromatic hydrocarbons from residential coal combustion in China, *Environmental Science & Technology*, 39,
533 1861-1867, 10.1021/es0493650, 2005.
- 534 Chen, Y., and Bond, T. C.: Light absorption by organic carbon from wood combustion, *Atmospheric Chemistry and*
535 *Physics*, 10, 1773-1787, 10.5194/acp-10-1773-2010, 2010.
- 536 Claeys, M., Vermeylen, R., Yasmeeen, F., Gómez-González, Y., Chi, X., Maenhaut, W., Mészáros, T., and Salma, I.:
537 Chemical characterisation of humic-like substances from urban, rural and tropical biomass burning environments
538 using liquid chromatography with UV/vis photodiode array detection and electrospray ionisation mass
539 spectrometry, *Environmental Chemistry*, 9, 273-284, <https://doi.org/10.1071/EN11163>, 2012.
- 540 De Haan, D. O., Hawkins, L. N., Welsh, H. G., Pednekar, R., Casar, J. R., Pennington, E. A., de Loera, A., Jimenez,
541 N. G., Symons, M. A., Zauscher, M., Pajunoja, A., Caponi, L., Cazaunau, M., Formenti, P., Gratién, A., Pangui,
542 E., and Doussin, J.-F.: Brown carbon production in ammonium- or amine-containing aerosol particles by reactive
543 uptake of methylglyoxal and photolytic cloud cycling, *Environmental Science & Technology*, 51, 7458-7466,
544 10.1021/acs.est.7b00159, 2017.
- 545 Desyaterik, Y., Sun, Y., Shen, X., Lee, T., Wang, X., Wang, T., and Collett, J. L.: Speciation of “brown” carbon in
546 cloud water impacted by agricultural biomass burning in eastern China, *Journal of Geophysical Research:*
547 *Atmospheres*, 118, 7389-7399, 10.1002/jgrd.50561, 2013.
- 548 Ding, Y., Pang, Y., and Eatough, D. J.: High-volume diffusion denuder sampler for the routine monitoring of fine
549 particulate matter: I. Design and optimization of the PC-BOSS, *Aerosol Science and Technology*, 36, 369-382,
550 10.1080/027868202753571205, 2002.

551 Di Lorenzo, R. A., and Young, C. J.: Size separation method for absorption characterization in brown carbon:
552 Application to an aged biomass burning sample, *Geophysical Research Letters*, 43, 458-465,
553 10.1002/2015gl066954, 2016.

554 Di Lorenzo, R. A., Washenfelder, R. A., Attwood, A. R., Guo, H., Xu, L., Ng, N. L., Weber, R. J., Baumann, K.,
555 Edgerton, E., and Young, C. J.: Molecular-size-separated brown carbon absorption for biomass-burning aerosol
556 at multiple field sites, *Environmental Science & Technology*, 51, 3128-3137, 10.1021/acs.est.6b06160, 2017.

557 Donahue, N. M., Epstein, S. A., Pandis, S. N., and Robinson, A. L.: A two-dimensional volatility basis set: 1. organic-
558 aerosol mixing thermodynamics, *Atmospheric Chemistry and Physics*, 11, 3303-3318, 10.5194/acp-11-3303-2011,
559 2011.

560 Feng, Y., Ramanathan, V., and Kotamarthi, V. R.: Brown carbon: a significant atmospheric absorber of solar
561 radiation?, *Atmospheric Chemistry and Physics*, 13, 8607-8621, 10.5194/acp-13-8607-2013, 2013.

562 Fleming, L. T., Lin, P., Laskin, A., Laskin, J., Weltman, R., Edwards, R. D., Arora, N. K., Yadav, A., Meinardi, S.,
563 Blake, D. R., Pillarisetti, A., Smith, K. R., and Nizkorodov, S. A.: Molecular composition of particulate matter
564 emissions from dung and brushwood burning household cookstoves in Haryana, India, *Atmospheric Chemistry
565 and Physics*, 18, 2461-2480, 10.5194/acp-18-2461-2018, 2018.

566 Forrister, H., Liu, J., Scheuer, E., Dibb, J., Ziemba, L., Thornhill, K. L., Anderson, B., Diskin, G., Perring, A. E.,
567 Schwarz, J. P., Campuzano-Jost, P., Day, D. A., Palm, B. B., Jimenez, J. L., Nenes, A., and Weber, R. J.: Evolution
568 of brown carbon in wildfire plumes, *Geophysical Research Letters*, 42, 4623-4630, 10.1002/2015gl063897, 2015.

569 Gilman, J. B., Lerner, B. M., Kuster, W. C., Goldan, P. D., Warneke, C., Veres, P. R., Roberts, J. M., de Gouw, J. A.,
570 Burling, I. R., and Yokelson, R. J.: Biomass burning emissions and potential air quality impacts of volatile organic
571 compounds and other trace gases from fuels common in the US, *Atmospheric Chemistry and Physics*, 15, 13915-
572 13938, 10.5194/acp-15-13915-2015, 2015.

573 Glarborg, P., Jensen, A., and Johnsson, J. E.: Fuel nitrogen conversion in solid fuel fired systems, *Progress in Energy
574 and Combustion Science*, 29, 89-113, 2003.

575 Global Alliance for Clean Cookstoves, 2014. Water Boiling Test (WBT) 4.2.3. Released 19 March 2014
576 <http://cleancookstoves.org/technology-and-fuels/testing/protocols.html> (accessed July 2017).

577 Harrison, M. A., Barra, S., Borghesi, D., Vione, D., Arsene, C., and Olariu, R. I.: Nitrated phenols in the atmosphere:
578 a review, *Atmospheric Environment*, 39, 231-248, 2005.

579 Hecobian, A., Zhang, X., Zheng, M., Frank, N., Edgerton, E. S., and Weber, R. J.: Water-soluble organic aerosol
580 material and the light-absorption characteristics of aqueous extracts measured over the Southeastern United States,
581 *Atmospheric Chemistry and Physics*, 10, 5965-5977, 10.5194/acp-10-5965-2010, 2010.

582 Iinuma, Y., Böge, O., Gräfe, R., and Herrmann, H.: Methyl-nitrocatechols: Atmospheric tracer compounds for
583 biomass burning secondary organic aerosols, *Environmental Science & Technology*, 44, 8453-8459,
584 10.1021/es102938a, 2010.

585 International Agency for Research on Cancer (IARC): Some non-heterocyclic polycyclic aromatic hydrocarbons and
586 some related exposures (Vol. 92). IARC Press, International Agency for Research on Cancer, 2010.

587 Jaekels, J. M., Bae, M. S., and Schauer, J. J.: Positive matrix factorization (PMF) analysis of molecular marker
588 measurements to quantify the sources of organic aerosols, *Environmental Science & Technology*, 41, 5763-5769,
589 10.1021/es062536b, 2007.

590 Jetter, J. J., and Kariher, P.: Solid-fuel household cook stoves: Characterization of performance and emissions,
591 *Biomass and Bioenergy*, 33, 294-305, <http://dx.doi.org/10.1016/j.biombioe.2008.05.014>, 2009.

592 Jetter, J., Zhao, Y., Smith, K. R., Khan, B., Yelverton, T., DeCarlo, P., and Hays, M. D.: Pollutant emissions and
593 energy efficiency under controlled conditions for household biomass cookstoves and implications for metrics
594 useful in setting international test standards, *Environmental Science & Technology*, 46, 10827-10834,
595 10.1021/es301693f, 2012.

596 Kaal, J., Martínez Cortizas, A., and Nierop, K. G. J.: Characterisation of aged charcoal using a coil probe pyrolysis-
597 GC/MS method optimised for black carbon, *Journal of Analytical and Applied Pyrolysis*, 85, 408-416,
598 <https://doi.org/10.1016/j.jaap.2008.11.007>, 2009.

599 Kim, K.-H., Jahan, S. A., Kabir, E., and Brown, R. J. C.: A review of airborne polycyclic aromatic hydrocarbons
600 (PAHs) and their human health effects, *Environment International*, 60, 71-80,
601 <https://doi.org/10.1016/j.envint.2013.07.019>, 2013.

602 Kim Oanh, N. T., Bætz Reutergårdh, L., and Dung, N. T.: Emission of polycyclic aromatic hydrocarbons and
603 particulate matter from domestic combustion of selected fuels, *Environmental Science & Technology*, 33, 2703-
604 2709, 10.1021/es980853f, 1999.

605 Kirchstetter, T. W., Corrigan, C. E., and Novakov, T.: Laboratory and field investigation of the adsorption of gaseous
606 organic compounds onto quartz filters, *Atmospheric Environment*, 35, 1663-1671, [https://doi.org/10.1016/S1352-](https://doi.org/10.1016/S1352-2310(00)00448-9)
607 2310(00)00448-9, 2001.

608 Klimont, Z., Cofala, J., Xing, J., Wei, W., Zhang, C., Wang, S., Kejun, J., Bhandari, P., Mathur, R., Purohit, P., Rafaj,
609 P., Chambers, A., Amann, M., and Hao, J.: Projections of SO₂, NO_x and carbonaceous aerosols emissions in
610 Asia, *Tellus B*, 61, 602-617, 10.1111/j.1600-0889.2009.00428.x, 2009.

611 Kwamena, N.-O., and Abbatt, J.: Heterogeneous nitration reactions of polycyclic aromatic hydrocarbons and n-hexane
612 soot by exposure to NO₃/NO₂/N₂O₅, *Atmospheric Environment*, 42, 8309-8314, 2008.

613 Lacey, F., and Henze, D.: Global climate impacts of country-level primary carbonaceous aerosol from solid-fuel
614 cookstove emissions, *Environmental Research Letters*, 10, 114003, 10.1088/1748-9326/10/11/114003, 2015.

615 Lei, Y., Zhang, Q., He, K. B., and Streets, D. G.: Primary anthropogenic aerosol emission trends for China, 1990–
616 2005, *Atmospheric Chemistry and Physics*, 11, 931-954, 10.5194/acp-11-931-2011, 2011.

617 Li, Q., Jacob, D. J., Bey, I., Yantosca, R. M., Zhao, Y., Kondo, Y., and Notholt, J.: Atmospheric hydrogen cyanide
618 (HCN): Biomass burning source, ocean sink?, *Geophysical Research Letters*, 27, 357-360,
619 10.1029/1999gl010935, 2000.

620 Lin, P., Aiona, P. K., Li, Y., Shiraiwa, M., Laskin, J., Nizkorodov, S. A., and Laskin, A.: Molecular characterization
621 of brown carbon in biomass burning aerosol particles, *Environmental Science & Technology*, 50, 11815-11824,
622 10.1021/acs.est.6b03024, 2016.

623 Lin, P., Bluvshstein, N., Rudich, Y., Nizkorodov, S. A., Laskin, J., and Laskin, A.: Molecular chemistry of atmospheric
624 brown carbon inferred from a nationwide biomass burning event, *Environmental Science & Technology*, 51,
625 11561-11570, 10.1021/acs.est.7b02276, 2017.

626 Lin, P., Liu, J. M., Shilling, J. E., Kathmann, S. M., Laskin, J., and Laskin, A.: Molecular characterization of brown
627 carbon (BrC) chromophores in secondary organic aerosol generated from photo-oxidation of toluene, *Physical
628 Chemistry Chemical Physics*, 17, 23312-23325, 10.1039/c5cp02563j, 2015.

629 Liu, J., Bergin, M., Guo, H., King, L., Kotra, N., Edgerton, E., and Weber, R. J.: Size-resolved measurements of brown
630 carbon in water and methanol extracts and estimates of their contribution to ambient fine-particle light absorption,
631 *Atmospheric Chemistry and Physics*, 13, 12389-12404, 10.5194/acp-13-12389-2013, 2013.

632 Lu, C., Wang, X., Li, R., Gu, R., Zhang, Y., Li, W., Gao, R., Chen, B., Xue, L., and Wang, W.: Emissions of fine
633 particulate nitrated phenols from residential coal combustion in China, *Atmospheric Environment*, 203, 10-17,
634 <https://doi.org/10.1016/j.atmosenv.2019.01.047>, 2019.

635 Lu, J. W., Flores, J. M., Lavi, A., Abo-Riziq, A., and Rudich, Y.: Changes in the optical properties of benzo[a]pyrene-
636 coated aerosols upon heterogeneous reactions with NO₂ and NO₃, *Physical Chemistry Chemical Physics*, 13,
637 6484-6492, 10.1039/C0CP02114H, 2011.

638 Lu, Z., Streets, D. G., Winijkul, E., Yan, F., Chen, Y., Bond, T. C., Feng, Y., Dubey, M. K., Liu, S., Pinto, J. P., and
639 Carmichael, G. R.: Light absorption properties and radiative effects of primary organic aerosol emissions,
640 *Environmental Science & Technology*, 49, 4868-4877, 10.1021/acs.est.5b00211, 2015.

641 McMeeking, G., Fortner, E., Onasch, T., Taylor, J., Flynn, M., Coe, H., and Kreidenweis, S.: Impacts of nonrefractory
642 material on light absorption by aerosols emitted from biomass burning, *Journal of Geophysical Research:*
643 *Atmospheres*, 119, 12,272-212,286, 2014.

644 Mohr, C., Lopez-Hilfiker, F. D., Zotter, P., Prévôt, A. S. H., Xu, L., Ng, N. L., Herndon, S. C., Williams, L. R.,
645 Franklin, J. P., Zahniser, M. S., Worsnop, D. R., Knighton, W. B., Aiken, A. C., Gorkowski, K. J., Dubey, M. K.,
646 Allan, J. D., and Thornton, J. A.: Contribution of nitrated phenols to wood burning brown carbon light absorption
647 in Detling, United Kingdom during winter time, *Environmental Science & Technology*, 47, 6316-6324,
648 10.1021/es400683v, 2013.

649 Nakayama, T., Matsumi, Y., Sato, K., Imamura, T., Yamazaki, A., and Uchiyama, A.: Laboratory studies on optical
650 properties of secondary organic aerosols generated during the photooxidation of toluene and the ozonolysis of α -
651 pinene, *Journal of Geophysical Research: Atmospheres*, 115, n/a-n/a, 10.1029/2010jd014387, 2010.

652 Park, R. J., Kim, M. J., Jeong, J. I., Youn, D., and Kim, S.: A contribution of brown carbon aerosol to the aerosol light
653 absorption and its radiative forcing in East Asia, *Atmospheric Environment*, 44, 1414-1421,
654 <https://doi.org/10.1016/j.atmosenv.2010.01.042>, 2010.

655 Peters, A. J., Lane, D. A., Gundel, L. A., Northcott, G. L., and Jones, K. C.: A comparison of high volume and diffusion
656 denuder samplers for measuring semivolatile organic compounds in the atmosphere, *Environmental Science &
657 Technology*, 34, 5001-5006, 10.1021/es000056t, 2000.

658 Pokhrel, R. P., Wagner, N. L., Langridge, J. M., Lack, D. A., Jayarathne, T., Stone, E. A., Stockwell, C. E., Yokelson,
659 R. J., and Murphy, S. M.: Parameterization of single-scattering albedo (SSA) and absorption Ångström exponent

660 (AAE) with EC / OC for aerosol emissions from biomass burning, *Atmospheric Chemistry and Physics*, 16, 9549-
661 9561, 10.5194/acp-16-9549-2016, 2016.

662 Ravindra, K., Sokhi, R., and Van Grieken, R.: Atmospheric polycyclic aromatic hydrocarbons: Source attribution,
663 emission factors and regulation, *Atmospheric Environment*, 42, 2895-2921,
664 <https://doi.org/10.1016/j.atmosenv.2007.12.010>, 2008.

665 Reff, A., Bhave, P. V., Simon, H., Pace, T. G., Pouliot, G. A., Mobley, J. D., and Houyoux, M.: Emissions inventory
666 of PM_{2.5} trace elements across the United States, *Environmental Science & Technology*, 43, 5790-5796,
667 10.1021/es802930x, 2009.

668 Riddle, S. G., Jakober, C. A., Robert, M. A., Cahill, T. M., Charles, M. J., and Kleeman, M. J.: Large PAHs detected
669 in fine particulate matter emitted from light-duty gasoline vehicles, *Atmospheric Environment*, 41, 8658-8668,
670 <https://doi.org/10.1016/j.atmosenv.2007.07.023>, 2007.

671 Saleh, R., Robinson, E. S., Tkacik, D. S., Ahern, A. T., Liu, S., Aiken, A. C., Sullivan, R. C., Presto, A. A., Dubey,
672 M. K., Yokelson, R. J., Donahue, N. M., and Robinson, A. L.: Brownness of organics in aerosols from biomass
673 burning linked to their black carbon content, *Nature Geoscience*, 7, 647-650, 10.1038/ngeo2220, 2014.

674 Samburova, V., Connolly, J., Gyawali, M., Yatavelli, R. L. N., Watts, A. C., Chakrabarty, R. K., Zielinska, B.,
675 Moosmüller, H., and Khlystov, A.: Polycyclic aromatic hydrocarbons in biomass-burning emissions and their
676 contribution to light absorption and aerosol toxicity, *Science of The Total Environment*, 568, 391-401,
677 <http://doi.org/10.1016/j.scitotenv.2016.06.026>, 2016.

678 Schneider, J., Bürger, V., and Arnold, F.: Methyl cyanide and hydrogen cyanide measurements in the lower
679 stratosphere: Implications for methyl cyanide sources and sinks, *Journal of Geophysical Research: Atmospheres*,
680 102, 25501-25506, 10.1029/97jd02364, 1997.

681 Shen, G., Tao, S., Wei, S., Zhang, Y., Wang, R., Wang, B., Li, W., Shen, H., Huang, Y., Chen, Y., Chen, H., Yang,
682 Y., Wang, W., Wei, W., Wang, X., Liu, W., Wang, X., and Simonich, S. L. M.: Reductions in Emissions of
683 Carbonaceous particulate matter and polycyclic aromatic hydrocarbons from combustion of biomass pellets in
684 comparison with raw fuel burning, *Environmental Science & Technology*, 46, 6409-6416, 10.1021/es300369d,
685 2012.

686 Shrivastava, M. K., Subramanian, R., Rogge, W. F., and Robinson, A. L.: Sources of organic aerosol: Positive matrix
687 factorization of molecular marker data and comparison of results from different source apportionment models,
688 *Atmospheric Environment*, 41, 9353-9369, 10.1016/j.atmosenv.2007.09.016, 2007.

689 Simoneit, B. R., Rogge, W., Mazurek, M., Standley, L., Hildemann, L., and Cass, G.: Lignin pyrolysis products,
690 lignans, and resin acids as specific tracers of plant classes in emissions from biomass combustion, *Environmental
691 science & technology*, 27, 2533-2541, 1993.

692 Simoneit, B. R.: Biomass burning—a review of organic tracers for smoke from incomplete combustion, *Applied
693 Geochemistry*, 17, 129-162, 2002.

694 Smith, K. R., Bruce, N., Balakrishnan, K., Adair-Rohani, H., Balmes, J., Chafe, Z., Dherani, M., Hosgood, H. D.,
695 Mehta, S., Pope, D., and Rehfuess, E.: Millions dead: How do we know and what does it mean? Methods used in
696 the comparative risk assessment of household air pollution, *Annual Review of Public Health*, 35, 185-206,
697 10.1146/annurev-publhealth-032013-182356, 2014.

698 Subramanian, R., Khlystov, A. Y., Cabada, J. C., and Robinson, A. L.: Positive and negative artifacts in particulate
699 organic carbon measurements with denuded and undenuded sampler configurations special issue of *Aerosol
700 Science and Technology* on findings from the fine particulate matter supersites program, *Aerosol Science and
701 Technology*, 38, 27-48, 10.1080/02786820390229354, 2004.

702 Sun, J., Zhi, G., Hitznerberger, R., Chen, Y., Tian, C., Zhang, Y., Feng, Y., Cheng, M., Cai, J., Chen, F., Qiu, Y., Jiang,
703 Z., Li, J., Zhang, G., and Mo, Y.: Emission factors and light absorption properties of brown carbon from household
704 coal combustion in China, *Atmospheric Chemistry and Physics*, 17, 4769-4780, 10.5194/acp-17-4769-2017, 2017.

705 Teich, M., van Pinxteren, D., Wang, M., Kecorius, S., Wang, Z., Müller, T., Močnik, G., and Herrmann, H.:
706 Contributions of nitrated aromatic compounds to the light absorption of water-soluble and particulate brown
707 carbon in different atmospheric environments in Germany and China, *Atmospheric Chemistry and Physics*, 17,
708 1653-1672, 10.5194/acp-17-1653-2017, 2017.

709 Tuccella, P., Curci, G., Pitari, G., Lee, S., and Jo, D. S.: Direct radiative effect of absorbing aerosols: sensitivity to
710 mixing state, brown carbon and soil dust refractive index and shape, *Journal of Geophysical Research:
711 Atmospheres*, 125, e2019JD030967, 10.1029/2019JD030967, 2020.

712 Turpin, B. J., and Lim, H.-J.: Species contributions to PM_{2.5} mass concentrations: Revisiting common assumptions
713 for estimating organic mass, *Aerosol Science and Technology*, 35, 602-610, 10.1080/02786820119445, 2001.

714 Wang, X., Heald, C. L., Ridley, D. A., Schwarz, J. P., Spackman, J. R., Perring, A. E., Coe, H., Liu, D., and Clarke,
715 A. D.: Exploiting simultaneous observational constraints on mass and absorption to estimate the global direct

716 radiative forcing of black carbon and brown carbon, *Atmospheric Chemistry and Physics*, 14, 10989-11010,
717 10.5194/acp-14-10989-2014, 2014.

718 Wathore, R., Mortimer, K., and Grieshop, A. P.: In-use emissions and estimated impacts of traditional, natural- and
719 forced-draft cookstoves in rural Malawi, *Environmental Science & Technology*, 51, 1929-1938,
720 10.1021/acs.est.6b05557, 2017.

721 Watson, J. G., Chow, J. C., Chen, L. W. A., and Frank, N. H.: Methods to assess carbonaceous aerosol sampling
722 artifacts for IMPROVE and other long-term networks, *Journal of the Air & Waste Management Association*, 59,
723 898-911, 10.3155/1047-3289.59.8.898, 2009.

724 Xie, M., Hannigan, M. P., Dutton, S. J., Milford, J. B., Hemann, J. G., Miller, S. L., Schauer, J. J., Peel, J. L., and
725 Vedal, S.: Positive matrix factorization of PM_{2.5}: Comparison and implications of using different speciation data
726 sets, *Environmental Science & Technology*, 46, 11962-11970, 10.1021/es302358g, 2012.

727 Xie, M., Hannigan, M. P., and Barsanti, K. C.: Gas/particle partitioning of n-alkanes, PAHs and oxygenated PAHs in
728 urban Denver, *Atmospheric Environment*, 95, 355-362, <http://dx.doi.org/10.1016/j.atmosenv.2014.06.056>, 2014.

729 Xie, M., Chen, X., Hays, M. D., Lewandowski, M., Offenbergl, J., Kleindienst, T. E., and Holder, A. L.: Light
730 absorption of secondary organic aerosol: Composition and contribution of nitroaromatic compounds,
731 *Environmental Science & Technology*, 51, 11607-11616, 10.1021/acs.est.7b03263, 2017a.

732 Xie, M., Hays, M. D., and Holder, A. L.: Light-absorbing organic carbon from prescribed and laboratory biomass
733 burning and gasoline vehicle emissions, *Scientific Reports*, 7, 7318, 10.1038/s41598-017-06981-8, 2017b.

734 Xie, M., Shen, G., Holder, A. L., Hays, M. D., and Jetter, J. J.: Light absorption of organic carbon emitted from
735 burning wood, charcoal, and kerosene in household cookstoves, *Environmental Pollution*, 240, 60-67,
736 <https://doi.org/10.1016/j.envpol.2018.04.085>, 2018.

737 Xie, M., Chen, X., Hays, M. D., and Holder, A. L.: Composition and light absorption of N-containing aromatic
738 compounds in organic aerosols from laboratory biomass burning, *Atmospheric Chemistry and Physics*, 19, 2899-
739 2915, 10.5194/acp-19-2899-2019, 2019.

740 Xie, M., Piedrahita, R., Dutton, S. J., Milford, J. B., Hemann, J. G., Peel, J. L., Miller, S. L., Kim, S.-Y., Vedal, S.,
741 Sheppard, L., and Hannigan, M. P.: Positive matrix factorization of a 32-month series of daily PM_{2.5} speciation
742 data with incorporation of temperature stratification, *Atmospheric Environment*, 65, 11-20,
743 <http://dx.doi.org/10.1016/j.atmosenv.2012.09.034>, 2013.

744 Yang, M., Howell, S. G., Zhuang, J., and Huebert, B. J.: Attribution of aerosol light absorption to black carbon, brown
745 carbon, and dust in China – interpretations of atmospheric measurements during EAST-AIRE, *Atmospheric
746 Chemistry and Physics*, 9, 2035-2050, 10.5194/acp-9-2035-2009, 2009.

747 Zhang, X., Lin, Y.-H., Surratt, J. D., and Weber, R. J.: Sources, composition and absorption Ångström exponent of
748 light-absorbing organic components in aerosol extracts from the Los Angeles basin, *Environmental Science &
749 Technology*, 47, 3685-3693, 10.1021/es305047b, 2013.

Table 1. Average concentrations of total NACs and tNAC_{OC}% in Q_f and Q_b samples by fuel type and WBT phase.

Fuel & Test phase	Red Oak		Charcoal	
	CS	HS ^a	CS	HS
Front filter (Q_f)				
Sample number	18	17 ^b	15	15
total NAC (µg m ⁻³)	3.43 ± 1.37	3.91 ± 2.06	0.51 ± 0.43	1.00 ± 0.48
tNAC _{OC} %	1.01 ± 1.06	0.98 ± 1.09	0.40 ± 0.25	0.31 ± 0.21
OC (µg m ⁻³) ^c	624 ± 410	908 ± 885	115 ± 72.0	447 ± 271
EC/OC ^c	1.74 ± 1.42	1.96 ± 1.74	6.12 ± 2.76	0.029 ± 0.012
Backup filter (Q_b)				
Sample number	18	17 ^b	14 ^b	15
total NAC (µg m ⁻³)	1.67 ± 0.76	1.79 ± 0.77	0.37 ± 0.31	1.30 ± 0.70
tNAC _{OC} %	3.31 ± 3.46	2.77 ± 2.66	1.10 ± 0.89	1.08 ± 0.51
OC (µg m ⁻³) ^c	78.4 ± 43.2	100 ± 58.4	41.9 ± 23.3	138 ± 70.8
Q_b/Q_f ratio (%)				
total NACs	50.8 ± 13.4	53.4 ± 26.2	84.1 ± 38.0	140 ± 52.9
OC ^c	14.8 ± 3.87	15.3 ± 6.37	35.4 ± 12.2	38.8 ± 18.9

^a Including three SIM phase samples from the 3-stone fire; ^b one filter sample was missed for analysis; ^c data were obtained from Xie et al. (2018).

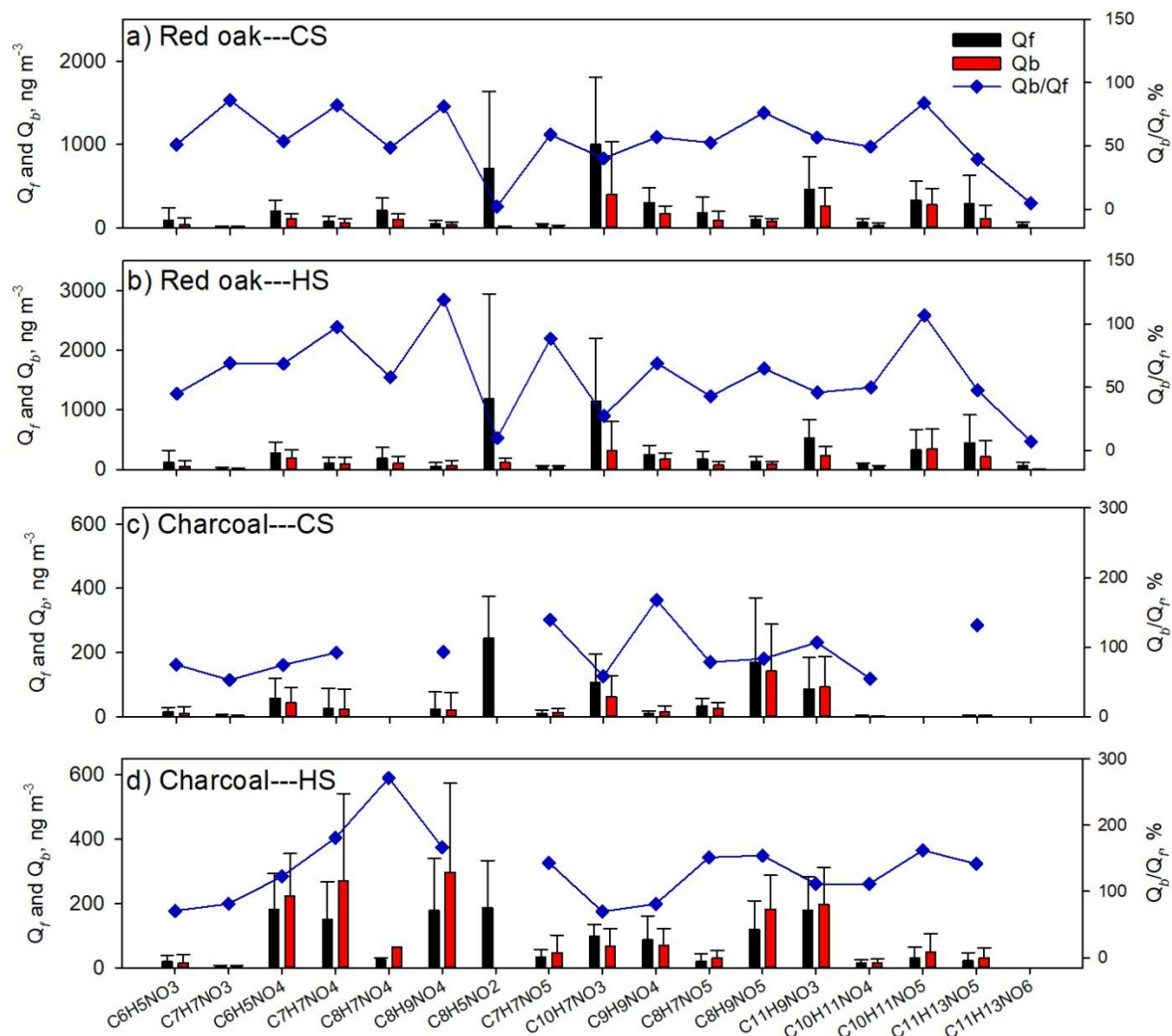


Figure 1. Average concentrations of individual NACs in Q_f and Q_b samples for (a) red oak burning under the CS phase, (b) red oak burning under the HS phase, (c) charcoal burning under the CS phase, and (d) charcoal burning under the HS phase. The blue scatters in each plot are mass ratios of individual NACs in Q_b to Q_f samples $\times 100\%$.

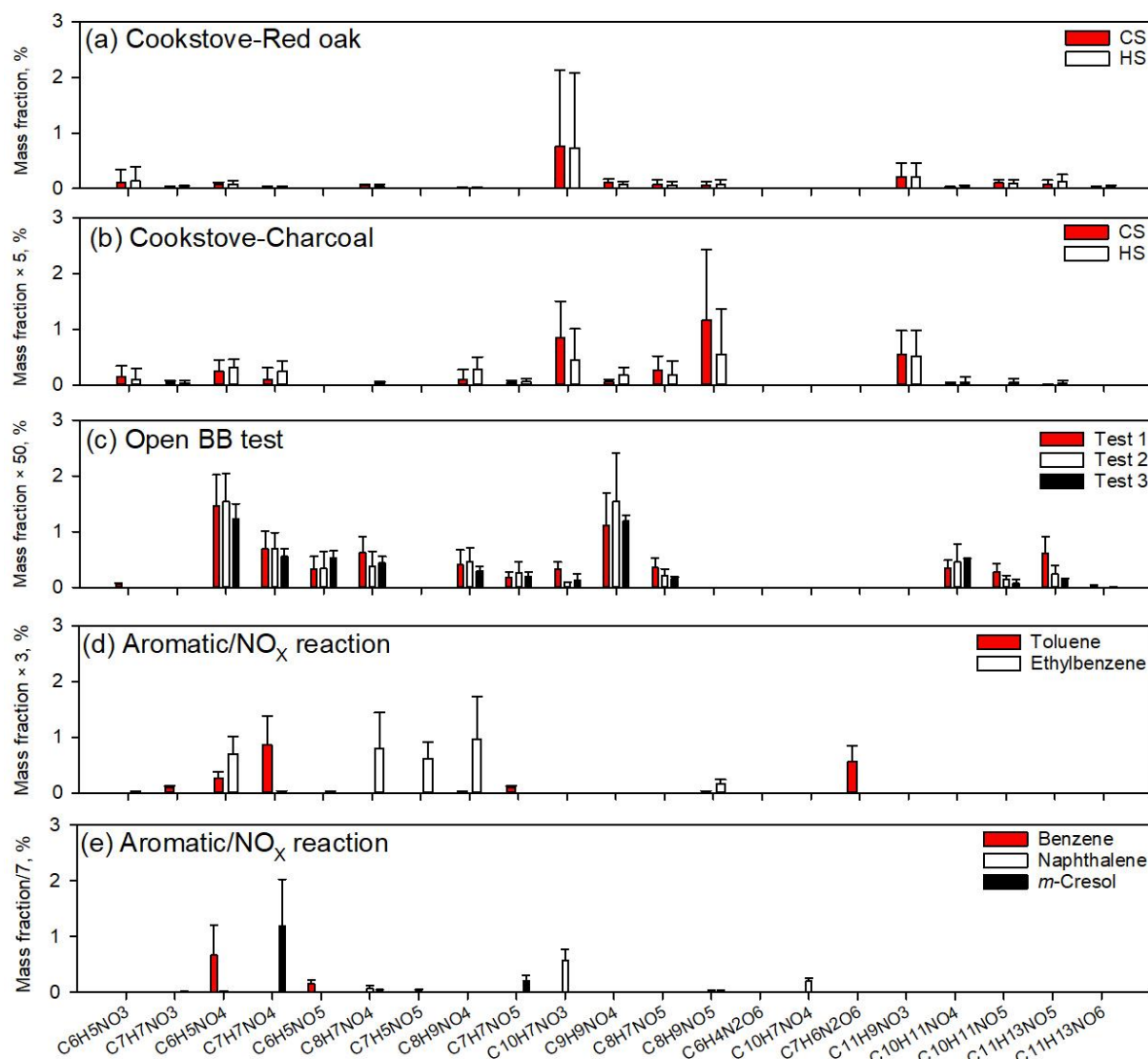


Figure 2. Average mass ratios (%) of individual NACs to organic matter from (a) red oak burning in cookstoves, (b) charcoal burning in cookstoves, (c) open BB experiments (Xie et al., 2019), photochemical reactions of (d) toluene and ethylbenzene, and (e) benzene, naphthalene, and m-cresol with NO_x (Xie et al., 2017a).

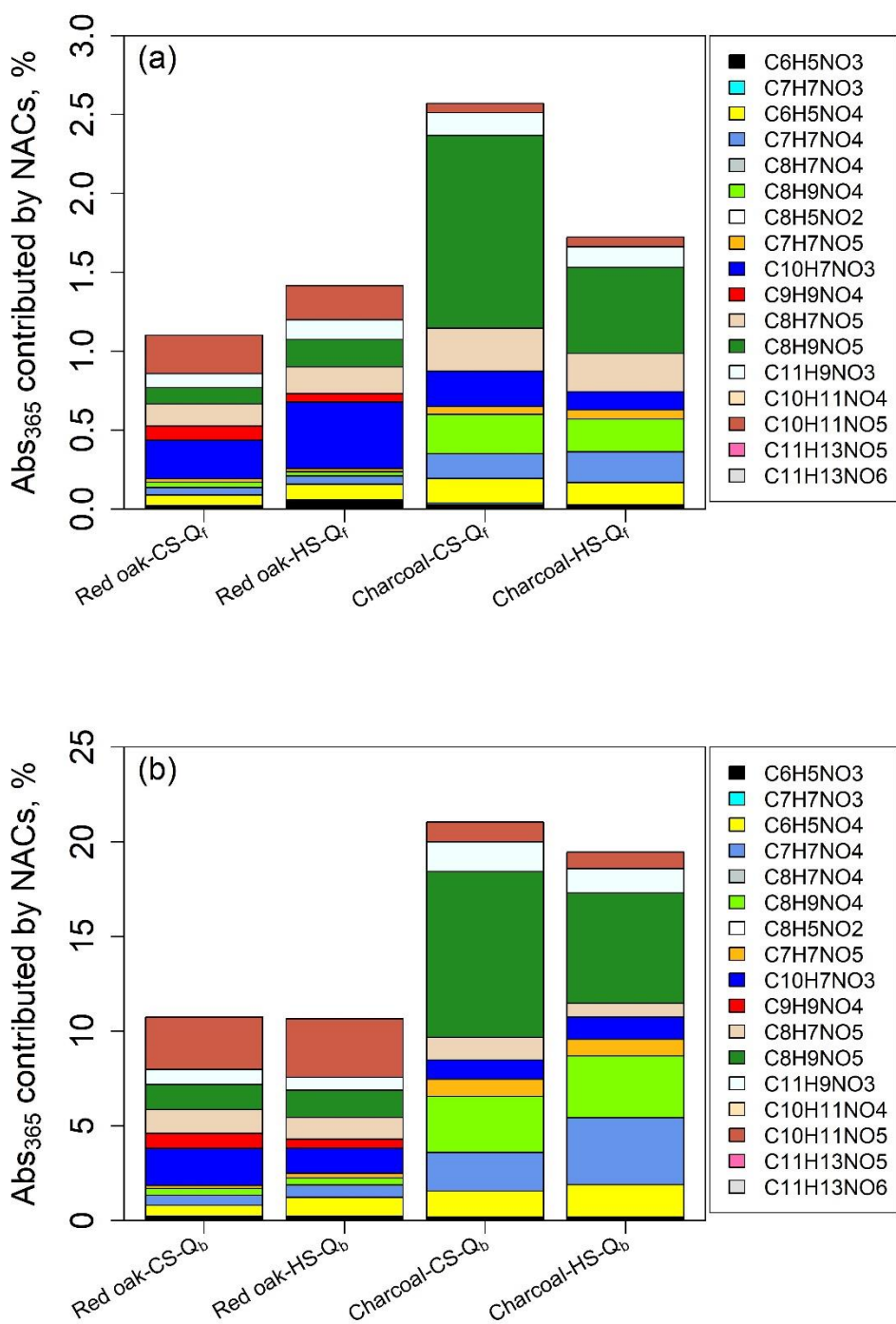


Figure 3. Average contributions (%) of individual NACs to bulk extracts Abs_{365} of (a) Q_f , and (b) Q_b samples from burning red oak and charcoal in cookstoves under CS and HS phases.